Aerolastic coupling and control means for reduction of main landing gear doors responses under operational conditions

Ramon Abarca, Carlo Aquilini, Pascal Lubrina, Shia Hui Peng, Jan Schwochow

International Forum on Aeroelasticity and Structural Dynamics
IFASD 2019
9-13 June 2019, Savannah, Georgia, USA

AEROLASTIC COUPLING AND CONTROL MEANS FOR REDUCTION OF MAIN LANDING GEAR DOORS RESPONSES UNDER OPERATIONAL CONDITIONS

R. Abarca[1], C. Aquilini[2], P. Lubrina[3], S.–H. Peng[4], J. Schwochow[5]

[1] AIRBUS Operations S.L.
28906 Getafe, Madrid, Spain
Ramon.Abarca@airbus.com

[2] AIRBUS Defense and Space
85077 Manching, Germany
Carlo.Aquilini@airbus.com

[3] ONERA
the French Aerospace Lab
92320 Châtillon, France
Pascal.Lubrina@onera.fr

[4] FOI Swedish Defence Research Agency
SE-16490 Stockholm, Sweden
Peng@foi.se

[5] German Aerospace Center (DLR)
37073 Goettingen,Germany
Jan.Schwohow@dlr.de

Keywords: buffet, landing gear doors, vibration control, flight test, ground vibration test

Abstract: Main landing gear doors cover the landing gear bays, keeping the aerodynamic shape of the aircraft during flight. They are open for the deployment and the retraction of the landing gears in the approach phase before landing and after take-off, respectively. During these phases, the nose landing gear creates flow separations, characterised by turbulent vortex motions, which are convected further downstream over the main landing gear region. This turbulent flow is responsible of unsteady aerodynamic loads on the main landing gear doors and may lead to vibrations (buffeting).
The present work summarises the key activities carried out in the frame of the European Project AFLoNext to characterise the structural response of the main landing gear doors of a commercial transport aircraft, as well as the effect of control devices designed, manufactured and flight-tested in order to mitigate their vibrations.

1 INTRODUCTION

Both nose landing gear (NLG) and main landing gear (MLG) systems in the aircraft undercarriage area are configured with structural components in complex layouts, including landing gear (LG) wheels, trunks, struts, housing-bay walls and LG doors. In the deployment for take-off or landing, these components are exposed to the external flow and generate vortex structures, responsible of dynamic loads. As a consequence, structural vibrations may be generated from the surface pressure fluctuations stemmed from the unsteady flow separation and/or from the extensive vortex motions. In order to validate and update the numerical modelling and simulations, ground and flight test activities were performed.
The structural response of the main landing gear doors (MLGDs) was characterised using a multi-physical approach. Section 2 provides a summary of the main results on the aircraft flow field and in particular in the NLG and MLGDs areas (see [1] and [2]). Unsteady CFD simulations were carried out using complete aircraft geometry, including representative LG, doors and cavities for different flight conditions. Section 3 describes the Ground Vibration Test (GVT) executed on the test aircraft, which provided the necessary key adjustments to the MLGD FEM in terms of eigenfrequencies, modal shapes and damping. The model update is

described in section 4. The aforementioned activities provided the inputs necessary for the buffeting analysis, described in detail in section 5.
CFD and buffeting analyses were important instruments for the design of devices able to reduce the structural vibrations of the MLGDs. These devices were designed, manufactured and finally flight-tested. Section 6 provides a brief description of the devices, of the flight test instrumentation (see also [3]) and of measurements results.

The next figure summarises all steps taken during the project, from the numerical predictions to the flight test. The related chapters are also highlighted.

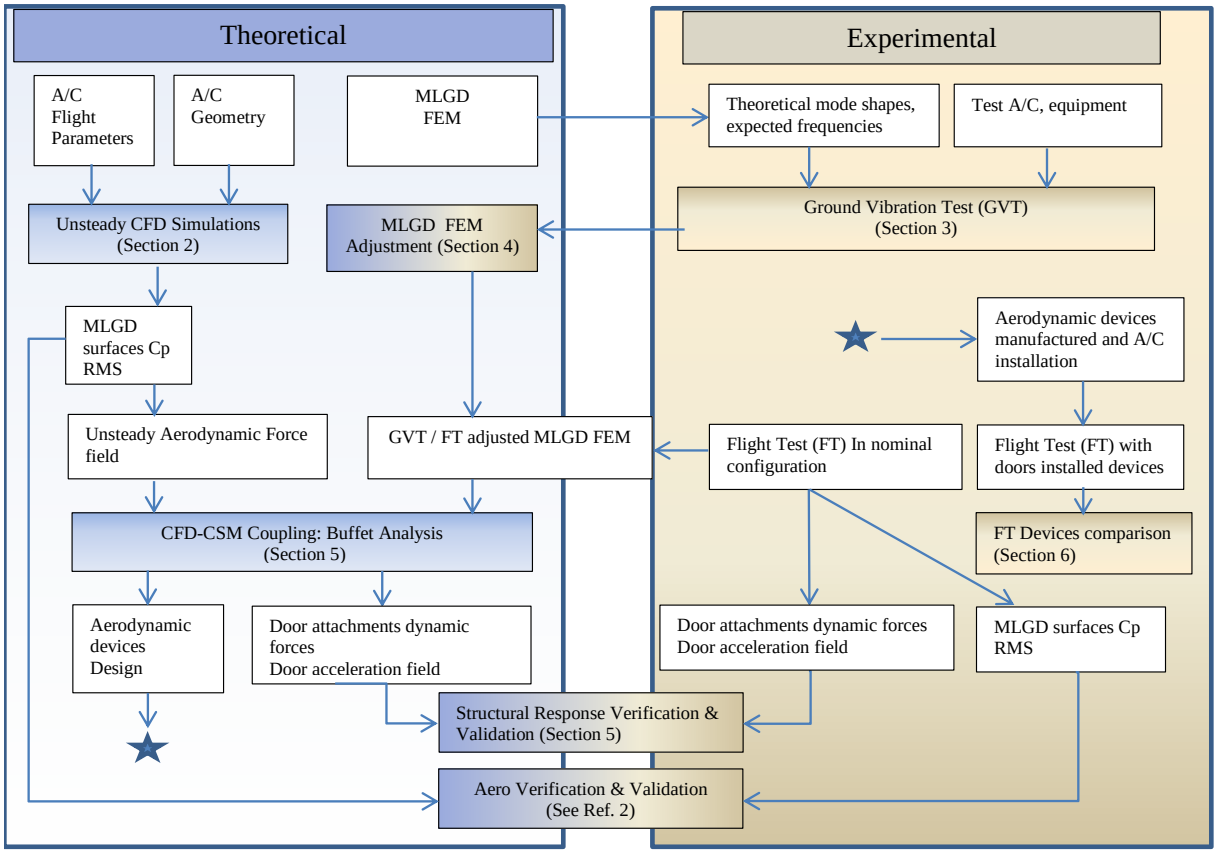

Figure 1: Process flow chart.

2 COMPUTATIONAL AERODYNAMIC ANALYSIS

In developing the technologies that allow mitigating vibrations in the undercarriage area, a comprehensive understanding on the aerodynamic loads acting on different components in this area must be proceeded first. This has been done by computational simulations and modelling with a particular focus on aerodynamic-flow-induced structural responses of the MLGDs in the deployment of MLGs. The aerodynamic analysis has targeted an exploration of the most influential dynamic response parameters and its connection/correlation with unsteady aerodynamic loads.

The overall goal was to identify main sources of flow unsteadiness that may generate vibrations in the MLGD structure. The major focus has thus been placed on, among others, (a) unsteady flow phenomena over the MLGD itself, (b) flows in proximity of the door, including the MLGs, the cavity bay and other structural components, (c) the vortices in the wake behind the NLG and washing over the MLGDs. In order to sort out the contributions from all these

sources, a systematic computational study was set in place that involves a number of steps to reach the final goal by a group of researchers in the AFLoNext project. Under a set of selected flight conditions, steady RANS (Reynolds-Averaged Navier-Stokes equations) solutions were produced on the flow around the aircraft with particular emphasis on the undercarriage area to highlight the flow properties around the MLGDs. The complex flow phenomena in the undercarriage area are characterized by turbulent flow separation and vortex motions, which are often unsteady and trigger aerodynamic flow fluctuations. The flow oscillations induce consequently unsteady aerodynamic loads on the MLGD and may lead to structural vibration.

Obviously, in order to predict the aerodynamic loads on the MLGDs and thus the associated structural responses, unsteady numerical simulations must be performed. Moreover, as mentioned, previous flight test has evidenced that, impacting on the MLGDs, the vortices generated by the NLG system has played a significant role in intensifying the MLGD unsteady aerodynamic loads. This suggests that the NLG-generated and down-washing vortex motion must be well resolved. With further refined grid resolution focusing on the undercarriage area, scale-resolving simulations have thus been conducted by involved partners using DES-type and other hybrid RANS-LES methods, as reported in, e.g., Peng *et al.* [1] and Tomac *et al.* [2]. The computations have reasonably resolved the vortex motion from the NLG to and after the MLG, as exampled in Figure 2. These computations have been carried out under a set of selected flight conditions for which the MLG and NLG are either fully or partially deployed/retracted. The unsteady pressures on the MLGD surfaces were sampled at each time step in every computation, which were then invoked in aeroelastic analysis of MLGD structural responses based on one-way CFD-CSM (Computational Structural Mechanics) coupling.

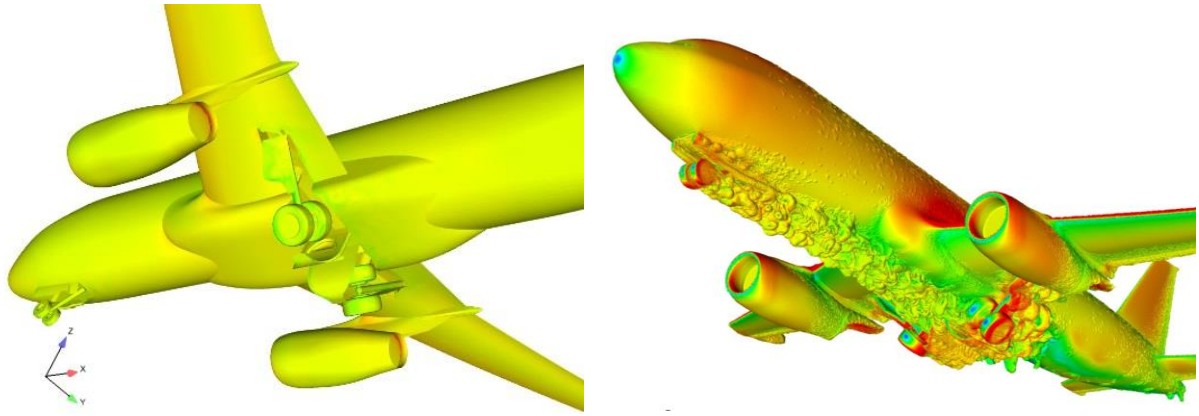

Figure 2: Example of scale-resolving CFD simulations of the flow in the undercarriage area from NLG to MLG.

Upon a systematic computational analysis, three main sources of aerodynamic excitation have been identified: the NLG wake, the MLG cavity flow and the flow separation over the MLGD surface (see Figure 3). A comprehensive exploration of the numerical simulations, and further in reference to the previous available flight test data, has shown that the extensive excitation of the MLGD comes when the landing gear on its half way is being deployed for landing or retracted after take-off. It is moreover evidenced with the computational analysis that the vortices in the NLG wake impacting on the main landing gear doors seem to be the most significant.

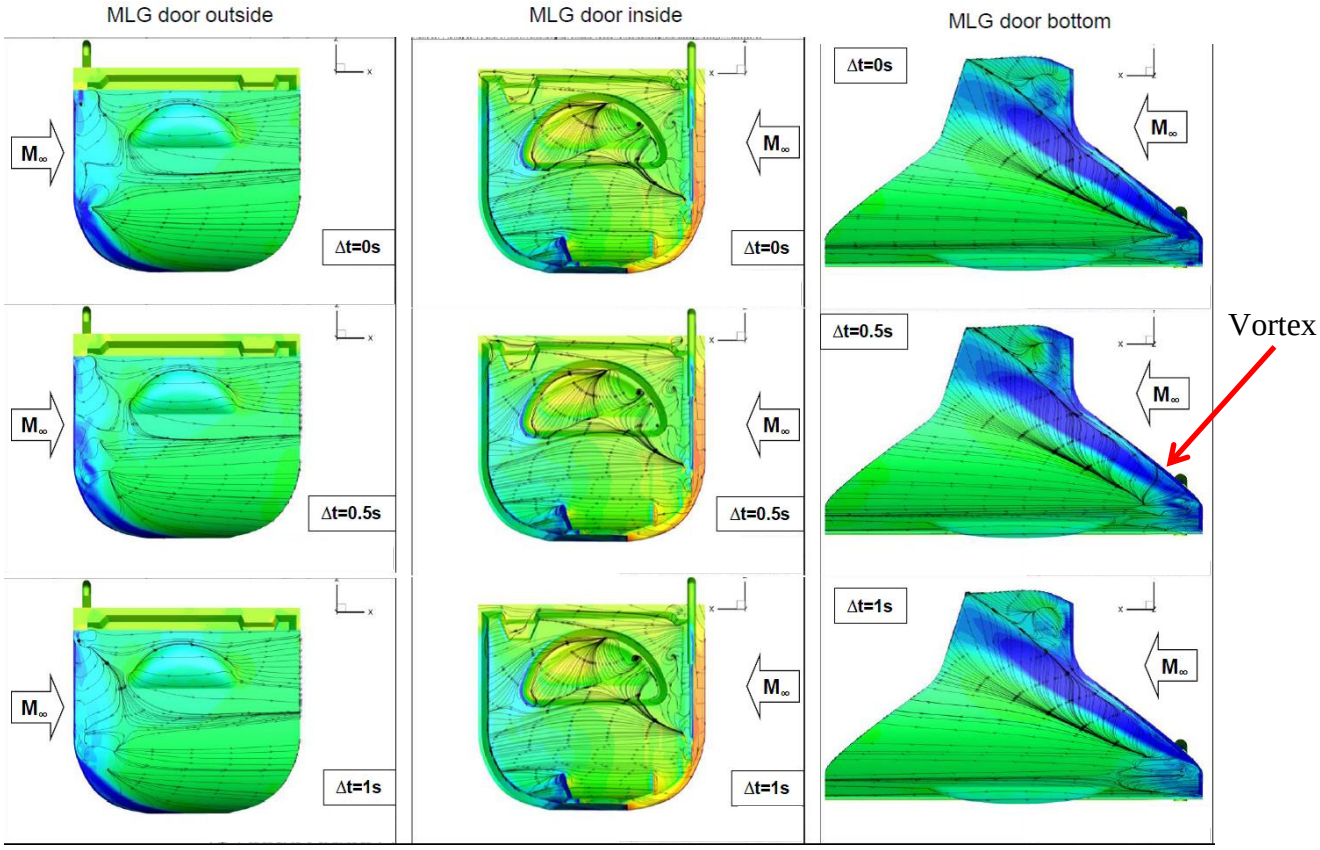

Figure 3: Example of time history distribution of the pressure coefficient Cp on the outer, inner and outer bottom face of the MLGD at landing conditions (see [2]).

3 GROUND VIBRATION TEST

A Ground Vibration Test focused on the left MLGD has been performed on the transport Aircraft "ATRA" owned by DLR. In order to update the FEM of the door, the objective of this test was to deliver the MLGD experimental modal characteristics, in its opened situation, attached to the aircraft. Three values of hydraulic pressure (nominal, median and null) in the actuator were tested.

Figure 4: View of the overall GVT installation.

Figure 5: GVT Vertical excitation view.

Both test methods, the Phase Resonance Method (PRM) and the Phase Separation Method (PSM) were applied. In addition to the 61 accelerometers installed on 21 sites on the door, 27 accelerometers were glued on 9 sites on the main aircraft structure (for instance on the wings

tip, engines and fuselage) reinforcing the observability of the complete dynamics, measuring also possible contributions of the aircraft.
Four different excitations locations/directions were necessary to excite sufficiently the door modes.

3.1 The Test Methods

The two typical methods for A/C GVT have been used: the PRM and PSM methods.

3.1.1 Phase Resonance Method

The PRM is applied to the vibration modes separately and it is reserved only to specific targeted modes, which exhibit or are propitious to exhibit a nonlinear behaviour. It is necessary to adjust in real time the frequency and the amplitudes of the sine excitation forces tuned in coincidence with the undamped resonance frequency of the target mode.

The PRM suits well to track nonlinear structural behaviours but it is time consuming. Therefore, it was originally planned to be used only for the first six modes and for the nominal configuration, by using only one exciter for each vibration mode.

The Forces in Quadrature method applied in PRM condition was initiated in the 50's and it is still considered by ONERA as one of the most reliable methods to determine structural damping coefficients and the generalized masses when using the PRM (see Figure 6). Starting from the tuned conditions (excitation frequency and force pattern), forces 90° shifted (i.e. forces in quadrature) are added sequentially. Those additional forces act as additional stiffness and then cause a deviation of the apparent resonance frequency. The damping ratio value of the mode is directly derived from those frequency deviations with respect to the amplitude of the imaginary parts of the introduced forces. Then the generalized mass can also be computed.

Software used: LMS TestLab NMT (Normal Mode Testing) workbook for PRM
ONERA GVT-Tool software to post process the PRM measurements

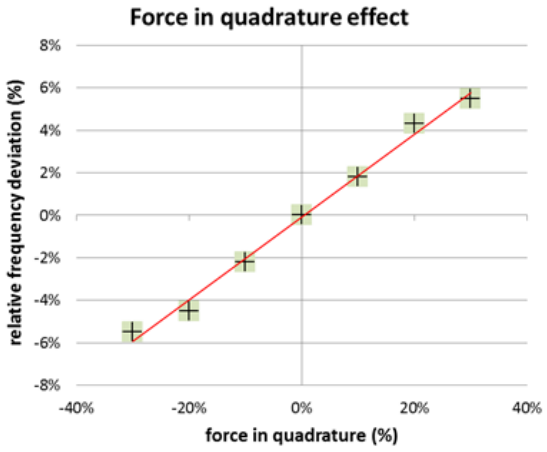

Figure 6: ONERA GVT tool environment. Example for Forces in Quadrature in PRM.

3.1.2 Phase Separation Method

For the PSM, we made use of the Siemens-LMS Polymax algorithm.

Software used: Siemens-LMS TestLab MIMO (Multi Inputs Multi Outputs) workbook
ONERA GVT-Tool software to design the excitation signal
ONERA GVT-Tool software to post-process the time measurements
Siemens-LMS LMS TestLab Polymax for the modal identification

Measurement examples perpendicular to the door excitation are shown in Figure 7 and Figure 8.

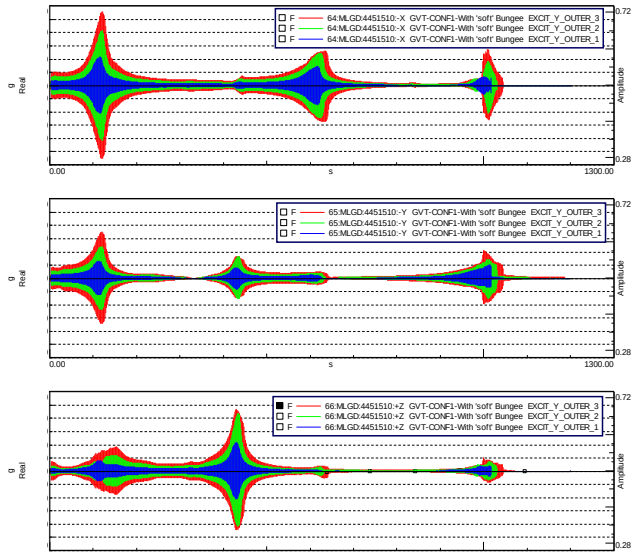

Figure 7: Time responses of 1 sensor from 3 force levels applied from 150Hz to 5 Hz.

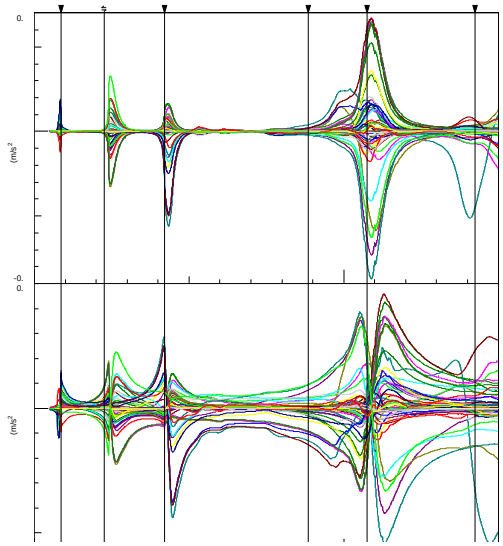

Figure 8: All measured FRFs (Vertical cursors correspond to the PRM resonance frequencies).

3.2 Installation of Bungee Cords

This technique is used by ONERA for 20 years, notably for the modal identification of landing gears. In order to cancel the existing free play in the hinges of the door and/or of the actuator, a long bungee cord was installed between the door and a fixed placed in the test hall, applying a quasi-static load adding a small additional stiffness (see Figure 9).

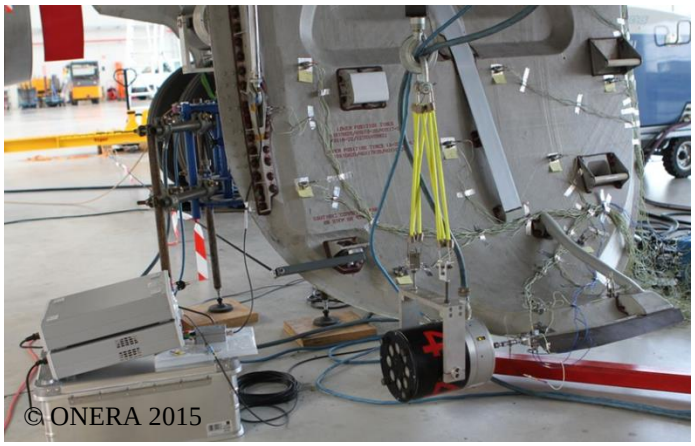

Figure 9: View of the bungee and the axial excitation.

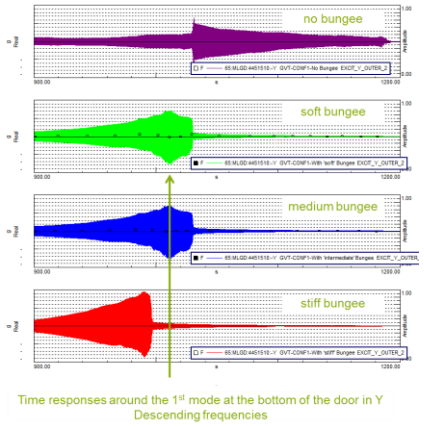

Figure 10: Time responses for several bungee conditions.

The very first measurements were dedicated to adjust the best bungee configuration (Figure 10, with a final setup having a free length of 6 m and a stiffness of 21N/m, measured with a load sensor). The absence or reduction of the free play reduces the nonlinear structural behaviour and then it makes possible the application of the PRM. This permits also a more reliable modal identification using with the Polymax algorithm. Remark: in flight conditions, the static aerodynamic forces on the door act similarly as the bungee installed on ground.

3.3 Ground Vibration Test Results

3.3.1 Mode Shapes

As an example, the first four modes are shown in Figure 11, measured with the PRM and PSM.

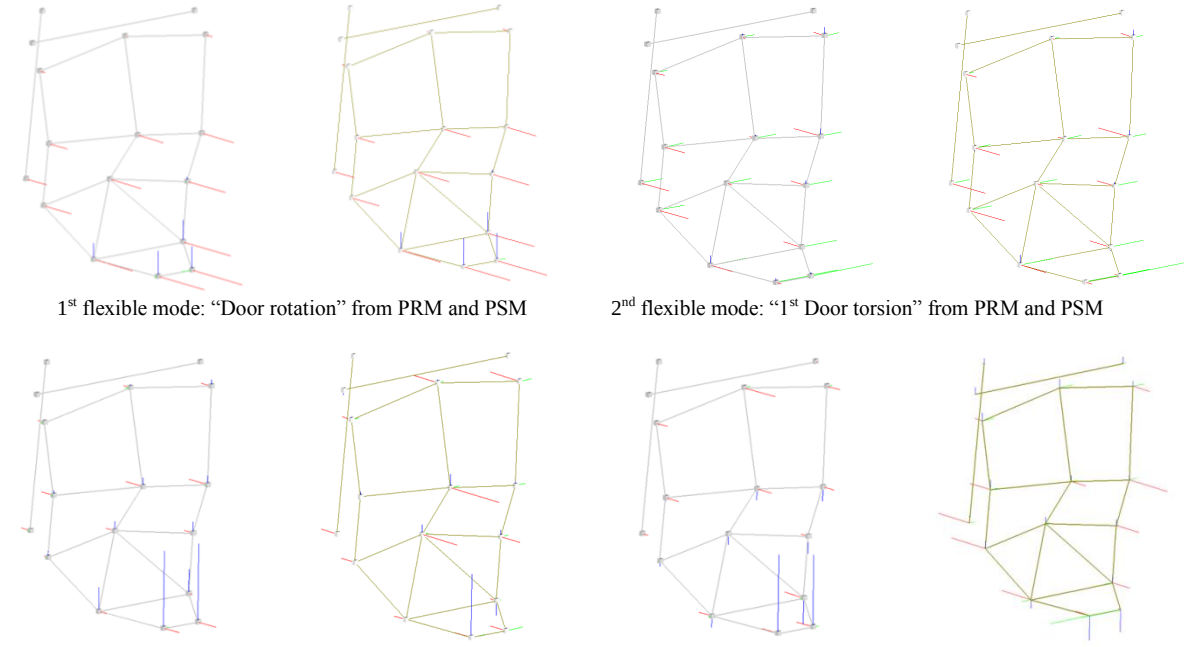

1st flexible mode: "Door rotation" from PRM and PSM

2nd flexible mode: "1st Door torsion" from PRM and PSM

3st flexible mode: "Door bending 1" from PRM and PSM

4th flexible mode: "Door bending 2" from PRM and PSM

Figure 11: The first four flexible door mode shapes identified with the PRM and PSM.

3.3.2 Mode Qualification

The Modal Assurance Criterion (MAC) is used to pair, as far as possible, the mode shapes between two mode families or inside a single family. In this case, the AutoMAC label is used. The MAC between the mode shape *n* and the mode shape *m* is defined as

$$MAC_{n,m} = \frac{\emptyset_n{}^T \times \emptyset_m}{|\emptyset_n|^2 \times |\emptyset_m|^2} \quad (1)$$

MAC = 100% (or 1 depending to the normalization used) when the mode shapes are strictly identical (see Figure 12 and Figure 13).

The Modal Indicator Function (Mif) quantifies the "purity" of the mode shapes and it is defined as

$$Mif_n = 1 - \frac{\sum(|imag(\emptyset_n)| \times |\emptyset_n|)}{\sum|\emptyset_n|^2} \quad (2)$$

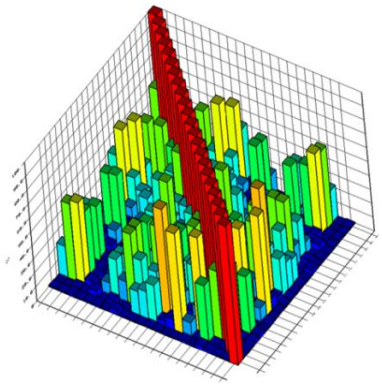

Figure 12: AutoMAC of 22 mode shapes identified from PSM. MAC=1 or 100% (red bars) means identical mode shapes. It is true on the diagonal and it is preferable to have blue or small bars elsewhere.

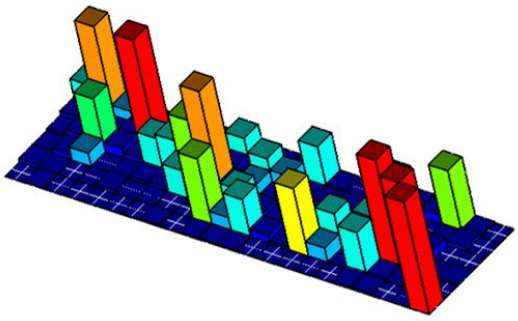

Figure 13: MAC between the 6 mode shapes measured by PRM and the 22 mode shapes measured from PSM. Four modes appear to be nearly identical (red bars), 2 comparable (orange bars).

$Ø_n$ is n-th mode shape; *real*($Ø_n$) transports the main part of the shape and *imag*($Ø_n$) gives the 'out of phase' contribution of the mode, due to the coupling with nearby modes or/and due to the lack of the Basile hypothesis of the mode $Ø_n$ (i.e. the hypothesis of orthogonality of the modal matrix is not valid). Mif = 1000 (or 1 or 100% depending to the normalization used) means that the mode is strictly real (see Figure 14).

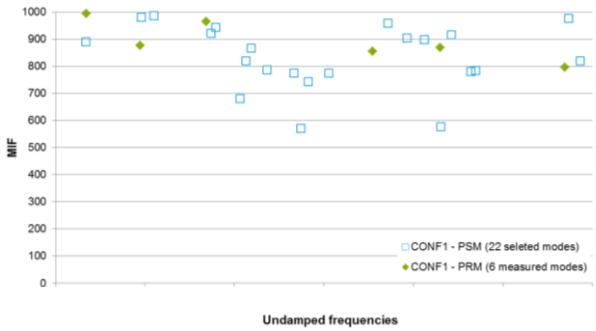

Figure 14: Modal Indicator Function of all PRM and PSM mode shapes.

3.3.3 Nonlinearity Plots

Since the excitation forces are applied at different locations and directions, the excitation power values are more pertinent for a valid comparison of the modal parameters. Figure 15 shows nonlinearity plots of the eigenfrequencies measured with the PRM.

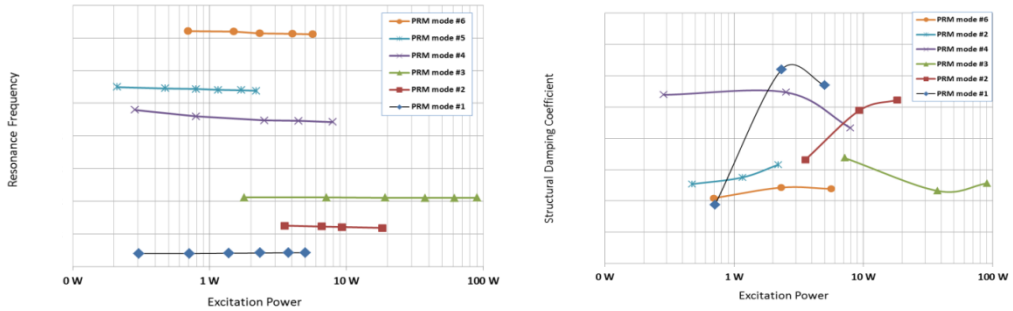

Figure 15: PRM resonance frequencies and structural damping coefficients versus excitation powers.

4 UPDATE OF THE FINITE ELEMENT MODEL

The GVT highlighted discrepancies between the dynamic behaviour of the tested MLGD from the original FEM. Differences of the numerical and measured eigenfrequencies are summarised in Figure 16. The root cause was identified in some additional aircraft stiffness, which participates on the front attachment of the MLGD. Obviously, this could not be considered in the analytic model of the isolated door. As a consequence, the FEM model required to be updated in order match the GVT results. The target was to match only the first three elastic modes of the door, which were thought to be the most relevant of the door structural dynamics during in flight. Anyway, after the model update, the MAC of the third mode continued to show a non-reliable matching (see Table 1). This will create discrepancies in the comparison of the buffeting numerical results with the flight test measurements in section 5.

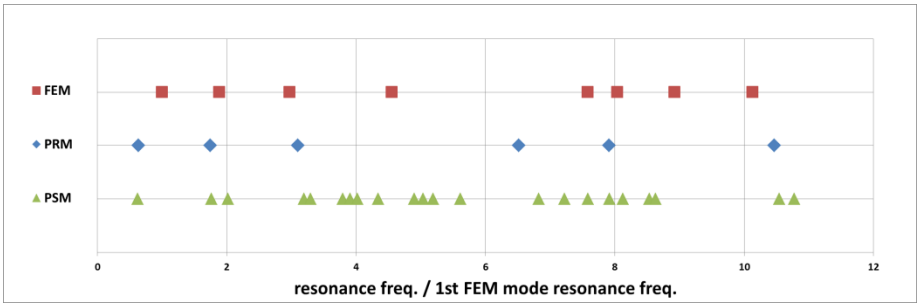

Figure 16: Comparison of FEM and GVT eigenfrequencies, before the model update.

Table 1: Comparison of FEM and GVT results, after the model update.

	Updated FEM (f/fref)	GVT (f/fref)	MAC
1st Mode: Rigid body rotation around hinge line	1.00	0.99	95.2 %
2nd Mode: Rigid body rotation body X-Z plane mode	2.87	2.75	80.6 %
3rd Mode: Elastic bending mode around hinge line	4.89	4.90	65.6 %

5 CFD-CSM COUPLING: THE BUFFETING ANALYSIS

The aeroelastic response of the structure to the unsteady flow excitation (namely buffeting) was computed in modal space using a stochastic approach. The theoretical background of the performed simulations is described in [4].

The aforementioned method is derived for wide-sense stationary stochastic processes. The starting point is the availability of the unsteady, motion-independent pressure distribution on a three-dimensional aerodynamic grid (either from CFD or from test measurements, obtained in flight or in wind tunnel) and a structural model. Depending on the nature of the problem, the self-induced aerodynamic forces could also have an important impact on the structural response and they are, therefore, to be included in the formulation. An industry standard within the field of the linear methods for the determination of the generalized aerodynamic forces is the doublet-lattice method (see [5]).

The transfer function of the aeroelastic system is described in modal space as (cf. [6])

$$\mathbf{H}(j\omega) = \left[-\omega^2\widetilde{\mathbf{M}} + j\omega\widetilde{\mathbf{B}} + (1+jg)\widetilde{\mathbf{K}} - q_\infty\widetilde{\mathbf{Q}}(Ma,k)\right]^{-1} \tag{3}$$

where ω is the circular frequency, $\widetilde{\mathbf{M}}$ the generalized mass, $\widetilde{\mathbf{B}}$ the modal damping, g the structural damping, $\widetilde{\mathbf{K}}$ the generalized stiffness, q_∞ the dynamic pressure, $\widetilde{\mathbf{Q}}(Ma, k)$ the generalized aerodynamic forces as function of the Mach number Ma and the reduced frequency k.
By using the transfer function $\mathbf{H}(j\omega)$, the modal matrix $\mathbf{\Phi}$ and the spectra of the aerodynamic excitation $\mathbf{S}_{f_g}(j\omega)$, the spectrum of the modal amplitudes $\mathbf{S}_\xi(j\omega)$ can be computed as

$$\mathbf{S}_\xi(j\omega) = \mathbf{H}(j\omega)\mathbf{\Phi}^\intercal \mathbf{S}_{f_g}(j\omega)\mathbf{\Phi}\mathbf{H}(j\omega)^\dagger \tag{4}$$

Physical displacements, velocities, accelerations and loads can then be easily obtained from the modal amplitudes (see [4]).

5.1 Buffeting of the Main Landing Doors

Buffeting analyses were performed using the unsteady pressure distributions obtained from CFD and the FEM updated with GVT test results (see previous sections).

5.1.1 The Structural Model

Since the steady aerodynamic excitation introduces a preloading to the door, which actually behaves stiffer than the current modelling, the actuator stiffness required further adjustment in order to match the eigenfrequencies seen in flight (further insight of the operational modal analysis can be found in [7]). The first four elastic modes of the model used for the buffeting analyses are shown in Figure 17. The modal damping coefficients measured during the GVT were used for the response analyses.

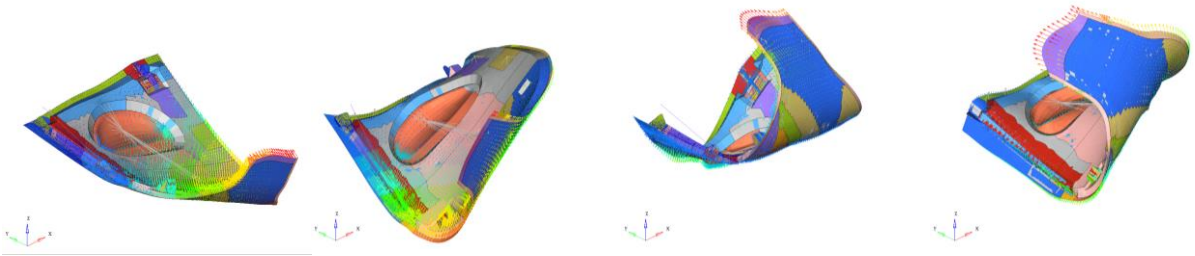

Figure 17: First four elastic modes of the FEM.

5.1.2 The Unsteady, Motion-Independent Pressure Distribution

A pre-processing to the CFD pressure data was needed before being able to run the buffeting simulations. First, the aerodynamic data was mirrored and transformed into the basic coordinate system of the FEM. The pressure signals were then down-sampled using the maximum resolution possible of the available signals. The mean components were removed and only the fluctuating parts of the input signals were considered. For simplicity, the door was shaped with six panels and the pressures were interpolated over a regular three-dimensional aerodynamic grid generated within these panels (by using a parametric bilinear surface, the hyperbolic paraboloid). This allowed to simplify the working chain and to speed-up the structural analyses. All aforementioned simplifications were considered acceptable, since main focus was in the frequency domain where the first three elastic modes of the FEM were matched with the GVT results.
Auto- and cross-spectra of the difference between the pressures on the outer and inner surfaces of the door were integrated obtaining a force distribution statically equivalent on the

aforementioned grid. Surface splines were then used in order to interpolate the spectra on the structural grid of the FEM (see [4]). Root-mean-squares (RMS) of the aerodynamic pressures and forces are shown in Figure 18. Once the spectra of the forces $\mathbf{S}_{f_g}(j\omega)$ were obtained on the FEM mesh, the buffeting problem in Eq. (4) could be solved.

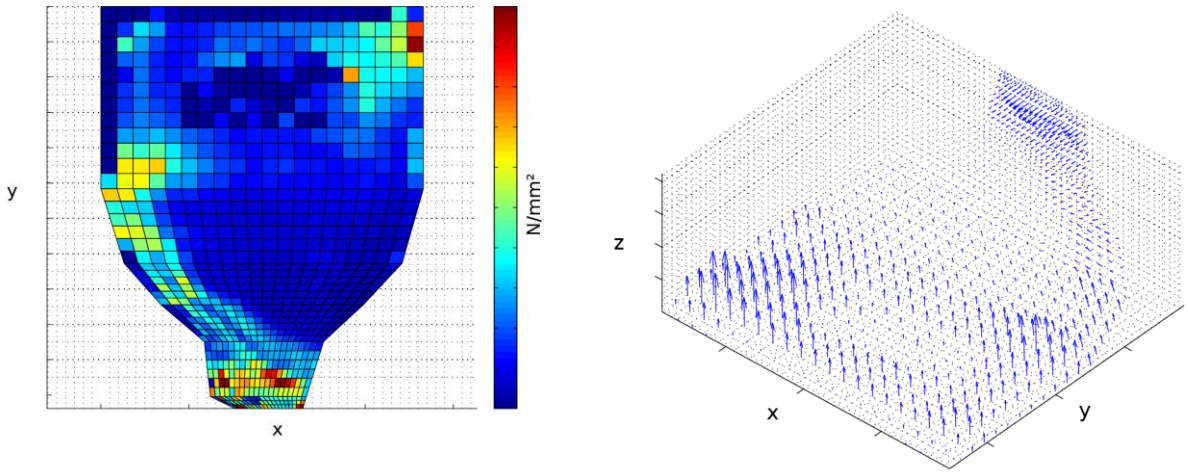

Figure 18: Root-mean-square of the pressures and forces on the aerodynamic grid. In the figure on the left aerodynamic grid is shown unfolded.

5.1.3 The Stochastic Analyses

Stochastic analyses were performed, obtaining accelerations at four nodes of the door as well as the reaction forces at the actuator fitting in terms of auto- and cross-spectra. The locations of the selected nodes are shown in Figure 19 and they are representative of the position of the sensors installed during the flight test activity (see also Figure 25).

Figure 19: Displacements and accelerations were computed on the four nodes on the left. Reaction forces were computed at the actuator fitting.

The results of the stochastic analyses are illustrated in Figure 20 and Figure 21 (red curve, square markers) together with measurements (blue curve, circle markers) in terms of power spectral densities of the actuator loads and accelerations, respectively.
Results clearly show the poor matching of the third elastic mode with GVT results (see section 4). On the other hand, the fourth elastic mode seems to be properly modelled. Excluding the third mode from the modal base and repeating the buffeting analysis sensibly improves the results at the hinge line location (see Figure 22).
RMS results of predictions and flight test measurements are shown in Table 2.

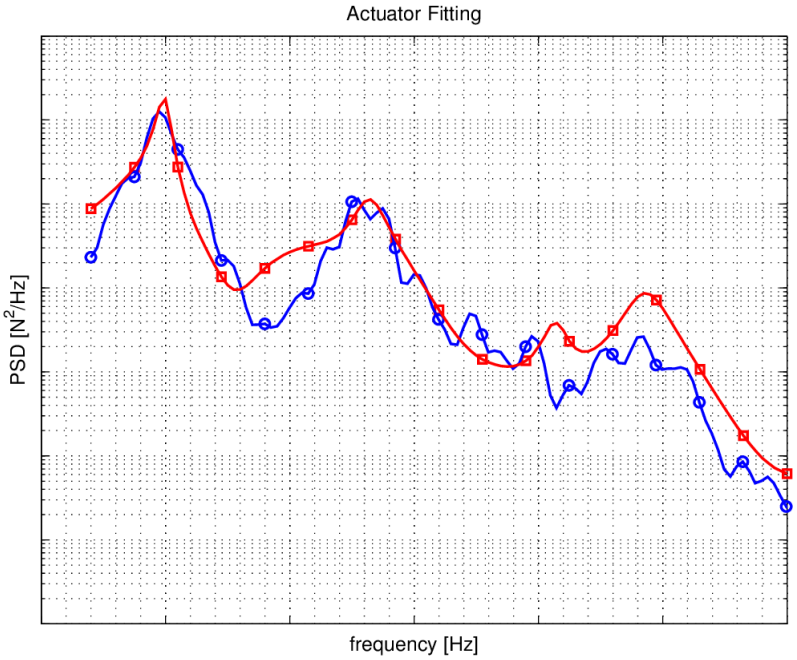

Figure 20: Numerical (red curve, square markers) and measured (blue curve, circle markers) PSD of the actuator loads.

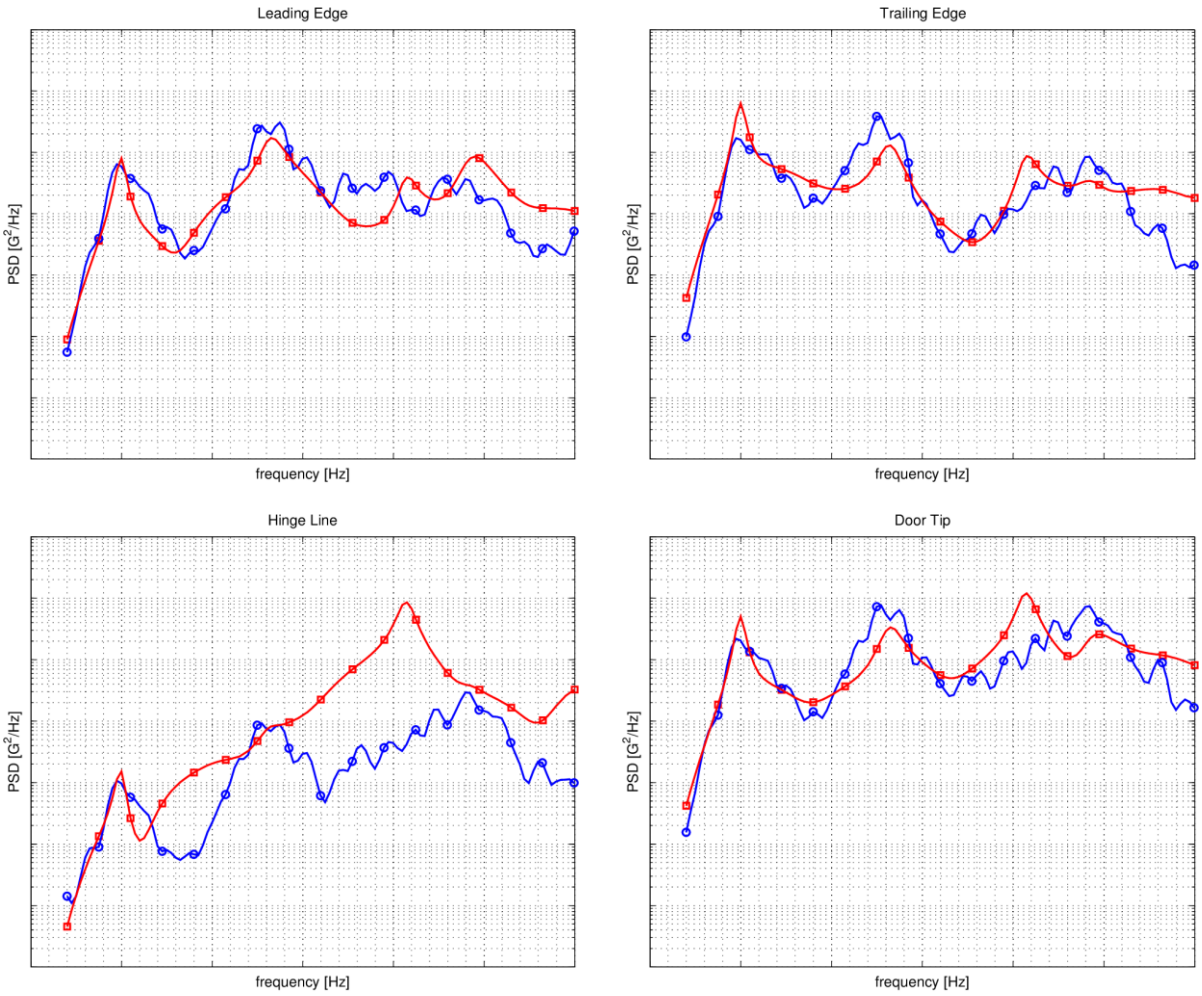

Figure 21: Numerical (red curve, square markers) and measured (blue curve, circle markers) PSD of the accelerations.

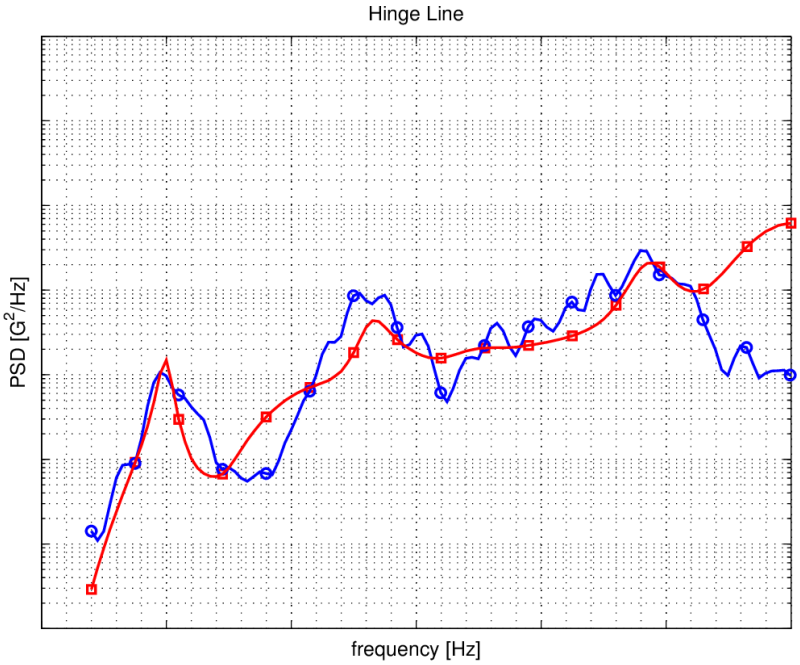

Figure 22: Numerical (red curve, square markers) and measured (blue curve, circle markers) PSD of the accelerations at the Hinge Line location.

Table 2: Comparison of predictions and flight test root-mean-square results.

	ΔRMS
Actuator	2.35 %
Leading Edge	-11.96 %
Trailing Edge	-2.47 %
Hinge Line	286.75 %
Hinge Line (excl. the 3th mode)	32.65 %
Door Tip	-0.61 %

6 CONTROL MEANS FOR STRUCTURAL RESPONSE REDUCTION

In order to reduce the structural response of the main landing gear doors when they are open during landing gear operations, the following devices were designed, manufactured and flight-tested: Vortex Generators (VGs), deflectors and a spoiler. The VGs were fitted on leading edge-outer doors faces, whilst the deflectors and the spoiler were installed on the leading edge-inner doors face (inside the landing gear cavity when the doors are closed).

6.1 The Theoretical Background

As described in section 2, the CFD analyses showed that the most significant impact on the aerodynamic excitation on the MLGDs depends from the NLG wake vortexes (see [2]) with a contribution of the flow separation from the doors leading edges (see [1]). The CFD analyses suggested that a mitigation of the structural vibrations could be achieved by manipulating the flow around the MLGDs and specifically by reducing the impact of the vortices convected from the NLG and by reducing the flow separation over the door surface.

6.1.1 The Vortex Generators

A mean to mitigate the aerodynamic excitation was to reduce the flow separation on the MLGD surfaces. VGs were appropriately installed on both sides of the MLGD. As shown in Figure 23, the surface flow separation could be effectively alleviated on both the inner and outer surfaces of the MLGD.

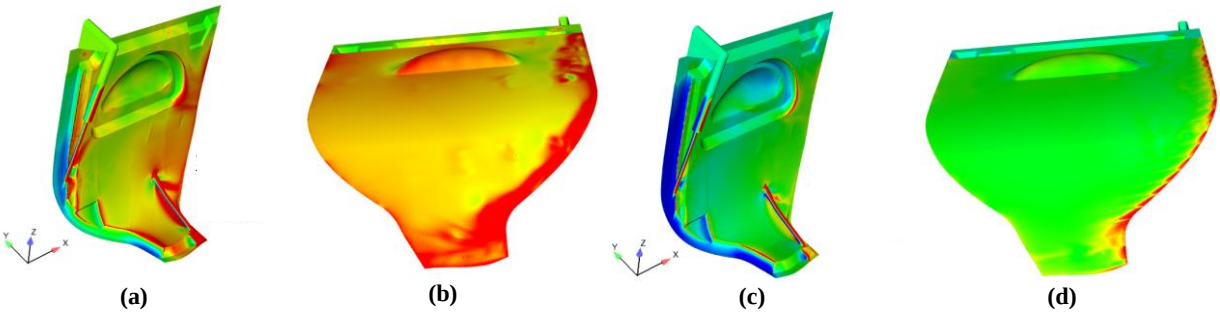

Figure 23: Resolved instantaneous pressures on the MLG door inner and outer surfaces, with/without flow separation control using VGs. (a) and (b) Clean configuration without vibration control on the MLGD. (c) and (d) Controlled configuration with VGs mounted on the MLGD surfaces.

The suppression of surface pressure fluctuations using VGs in computational analysis is further highlighted in Figure 24. The pressure fluctuations and their power-spectra relative to one point at the MLGD tip are compared for the cases with and without VGs, respectively. At this location, the computations showed that the VGs are actually able to mitigate the surface aerodynamic excitations over a wide span of frequencies and, therefore, they could be also used as Vibration Control (VC) devices.

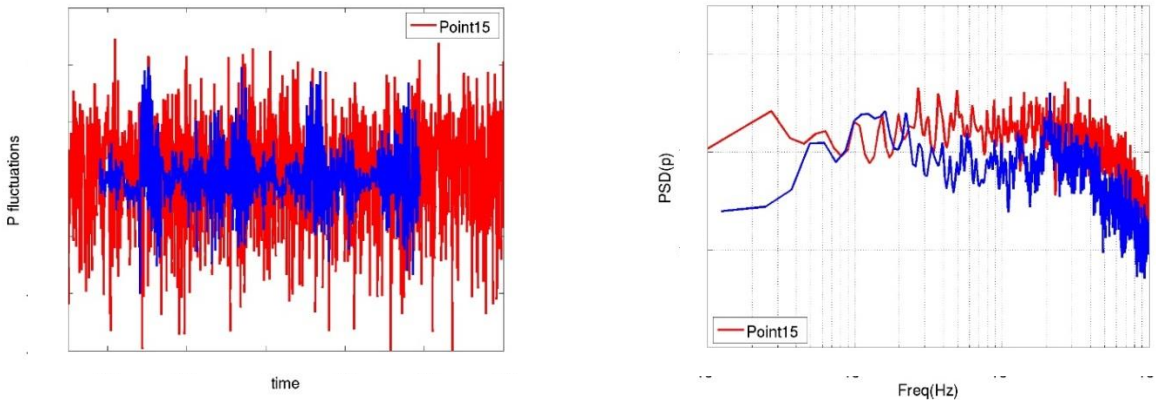

Figure 24: CFD pressure fluctuations at the MLGD tip. Computations for the baseline-configuration (red line) and configuration with VGs (blue line). (a) Pressure fluctuations; (b) PSD of pressure fluctuations as a function of frequency. Red line: Baseline case; Blue line: VGs adopted for vibration control.

6.1.2 The Deflectors

The deflectors are flat plates installed on the door leading edge, which reduce the magnitude of the local suction peak. The analysis of the time evolution of the local angle of attack obtained from CFD showed that high alternate suction peak variations occur on the door leading edge. If the geometry of the leading edge is modified in order to be less sensible to variations of the local angle of attack, then the magnitude of the suction peak can be reduced. Consequently the unsteady net pressure forces can also be reduced. Figure 26 shows the installation of the deflectors on the MLGD.

6.1.3 The Spoiler

The spoiler is a lifting surface installed on the door leading edge, with the scope to balance aerodynamically the door, reducing its tendency to open when the LG is in transit. As a consequence, a reduction of the structural response is expected to be achieved. Figure 26 shows the installation of the spoiler on the MLGD.

6.2 The Flight Test Instrumentation and the Flight Sequence

The instrumentation on the flight test A/C was comprehensive of several sensors installed on the MLGDs. Unsteady pressure sensors, accelerometers and strain gauges on the hydraulic actuator were installed on both MLGDs. This actuator is responsible to open, close and maintain the doors fully open during the landing gear operations. Figure 25 illustrates the flight test instrumentation (FTI) on one MLGD (see [3] and [7] for further details).

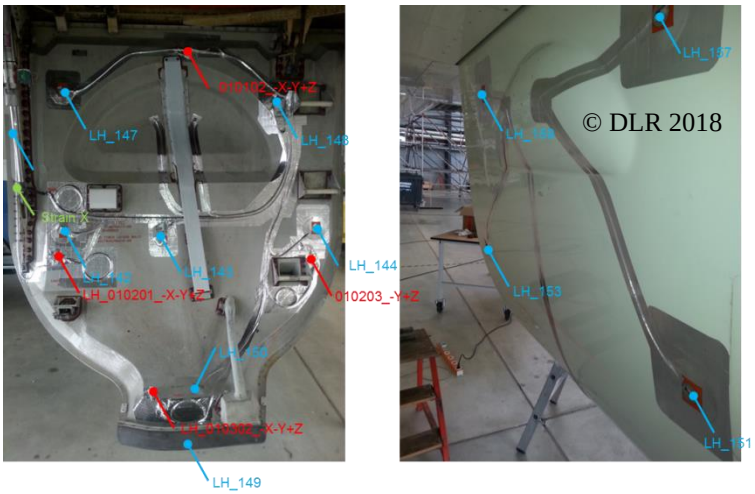

Figure 25: Accelerometers (red), Pressure transducers (blue), Actuator force (green) (see [3] and [7]).

Additionally to the FTI, the three devices were also installed on the MLGD (see Figure 26). The installation was done sequentially along the flight test campaign. First a reference flight was performed with no devices installed (in clean or baseline configuration); then a second flight was done with the VGs installed on both doors; finally, a third flight was performed with the spoiler fitted on the right hand door and the deflectors installed on the other one. It was demonstrated from flight test measurements that no mutual influence was produced between the devices fitted on the two doors.

Figure 26: Main Landing Gear Doors device installation on Flight Test A/C (see [3]).

6.3 The Flight Test Results

The flight test activities were performed under real operational conditions expected from normal airline usage in order to be representative of real in-service usage. Figure 27 describes one example of the landing gear deployment time sequence with the relative landing gear positions, door's actuator force, accelerations and pressures (cf. [3] and [7]). The doors structural response is amplified when the NLG is partially and then fully deployed.

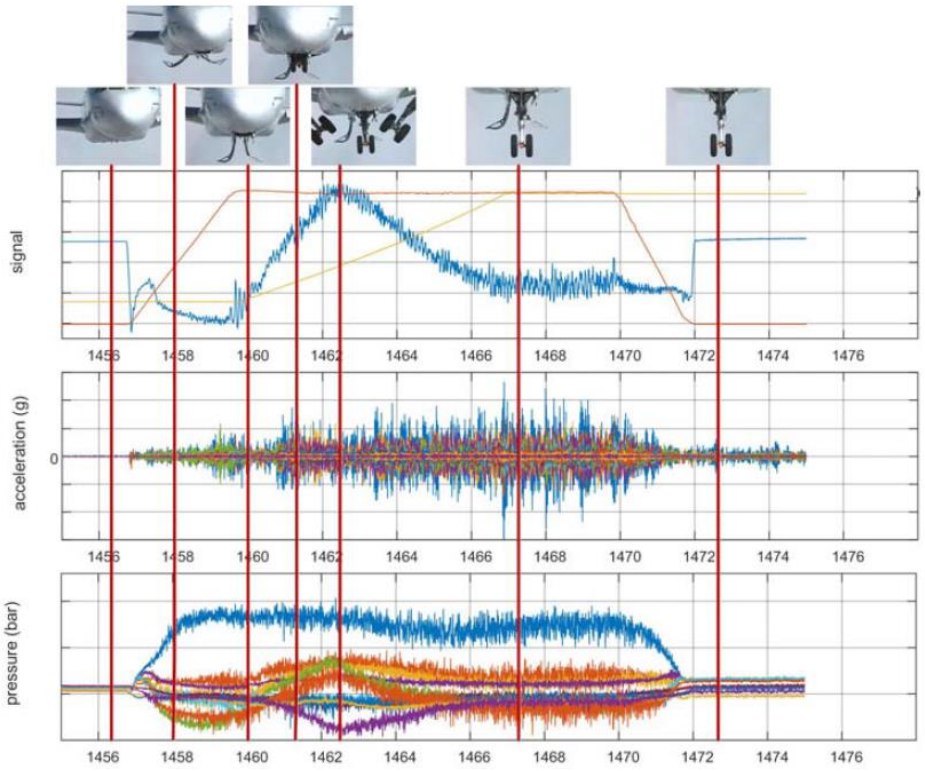

Figure 27: Main Landing Gear Doors Flight Test data example (see [3] and [7]).

As already mentioned, the MLGD is operated by a hydraulic actuator. Taking as loads reference the actuator force, systematic comparisons between the actuator force times histories were performed, in clean condition and with the devices installed. This was performed for the closest flight parameters. As an example, Figure 28 shows the superimposed time histories of the actuator force signals, for the same flight speed and at zero A/C side slip angle. The doors were fully open and the LG was in transit. This time window was selected for the comparison of the force signals of the configurations with devices and baseline. Examples of comparisons between the actuator force RMS time evolutions (overlapped time windows) are also shown in Figure 29 for low and high flight speeds. VGs and deflectors presented lower RMS levels than the clean configuration demonstrating the effective vibration reduction. The spoiler presented results, which were highly dependent from the flight speed, resulting almost ineffective at low speeds. Needs to be noted that structural responses between left hand (LH) and right hand (RH) sides are not the same (i.e.: clean condition). This is due to the fact that the unsteady NLG air-wake excitation is not symmetric.

Table 3 provides the RMS reduction achieved by each device compared with the clean condition. A global 10% reduction could be achieved consistently by VGs and deflectors. On the other hand, the effectiveness of the spoiler was highly dependent on the dynamic pressure.

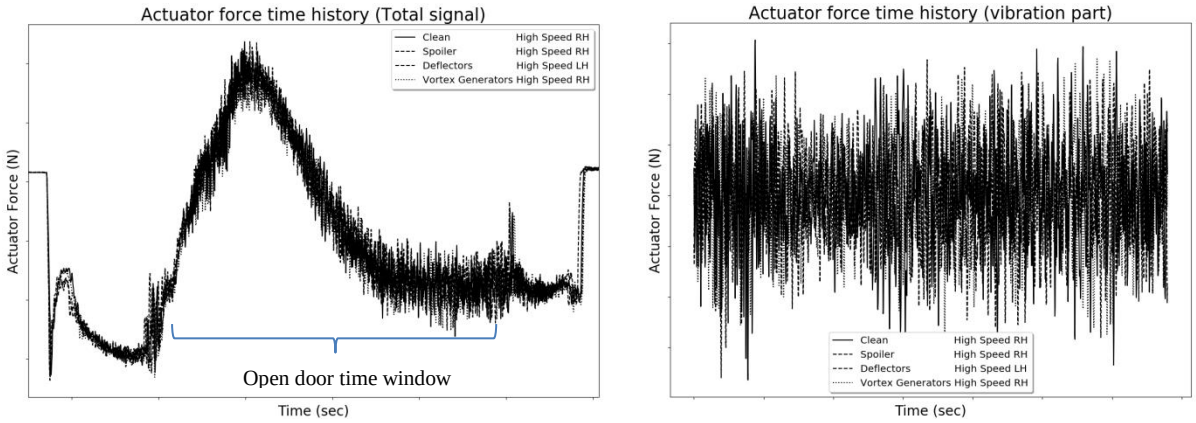

Figure 28: Actuator force time evolution. Left: Total signal, Right: Open door time window vibration.

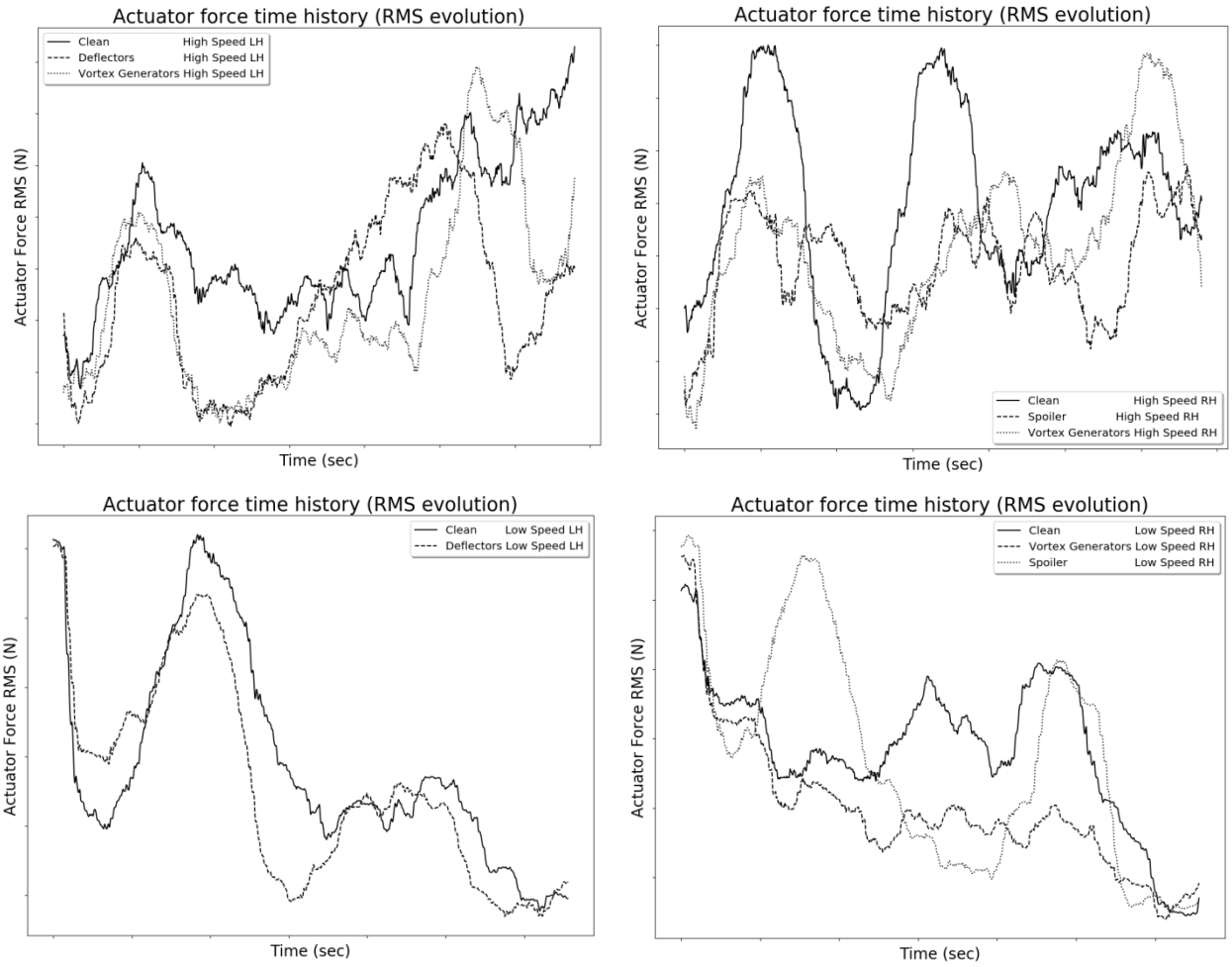

Figure 29: Actuator force RMS time evolution. Comparison between clean and configurations with devices.

Table 3: Comparison of the actuator force RMS values between clean and configurations with devices.

% of Actuator force RMS reduction with equipped device / clean (Flight Test)	Low A/C Speed	High A/C Speed
Vortex Generators	10.2 %	10.6 %
Deflectors	9.7 %	12.5 %
Spoiler	0.5 %	11.2 %

Figure 30 shows a comparison between the accelerations at the door tip (cf. Figure 25) for the clean condition and for the configuration with VGs devices. The predictions are illustrated in Figure 30a and the flight test measurements in Figure 30b.
The influence of the flow control on the MLGD deformations was evaluated by means of structural analyses by using the unsteady pressure excitation computed with unsteady CFD simulations. The results indicated that the high deformations of the structure were predominantly caused by the first mode at low frequencies. At such frequencies, flow control could substantially reduce the structural deformations. For example, at the lowest point on the door where the deformation was also the largest one, in the numerical simulation the reduction of the deformation due to flow control was estimated to be about 70% (see Figure 30(a)), while in the flight test measurements (with a relatively small angle of attack) the reduction was about 40% (see Figure 30(b)). The qualitative similarities between measurements and CFD-CSM simulations also demonstrated that the physics of the problem was fully captured.

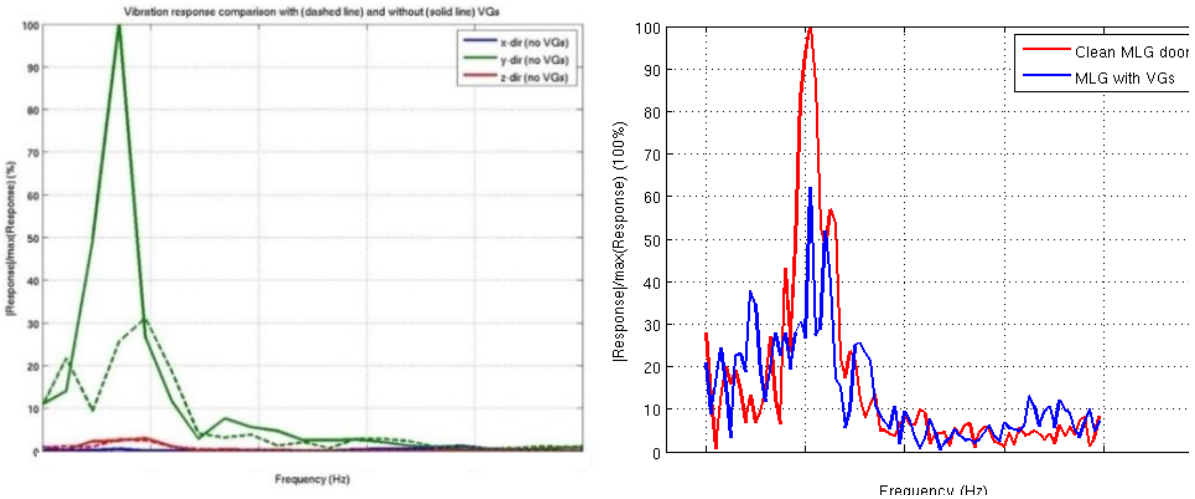

(a) (b)

Figure 30: Comparative analysis of VC effectiveness. (a) CFD-CSM results: Normalized frequency response of MLGD with VGs (dashed lines) and for the clean door (solid lines). (b) FT results: normalized frequency response of MLGD with VGs (blue line) and for clean door (red line).

7 CONCLUSIONS

Extensive research on the structural response of MLGDs under operational conditions of a typical landing gear tricycle configuration was presented and discussed.
Main objectives were first to characterise the structural response of the MLGDs from a theoretical point of view; secondly, to design control means for reducing their structural vibrations; finally, to validate the numerical modelling and assess the performance of the devices by means of flight test activities. This work is therefore a mixture of experimental and theoretical studies carried out in order to tackle this complex problem.

Peng *et al.* [1] and Tomac *et al.* [2] performed unsteady aerodynamic simulations of the complete aircraft with landing gears partial and fully deployed. This provided the necessary insight on the flow features that affect the pressure fluctuations on the MLGD. These studies showed that when the MLGDs are open and the landing gear is down in normal operation, the nose landing gear wake is the main source of the aerodynamic excitation of the MLGD. The second source is the flow separation on the MLGD leading edge and its interaction with the first source. Flight test measurements also confirmed this thesis. The CFD analyses provided

two parallel lines of investigation. On the one hand, they provided the unsteady pressure distributions under operational conditions, input for the buffeting simulations. On the other hand, they initiated the aerodynamic design of the control means for the reduction of the structural vibrations. Moreover, the outcome of the first line of investigation allowed also assessing the performance of these control means from a theoretical point of view.

A GVT on the MLGD was performed in order to measure its modal parameters. Both PSM and PRM were employed on the test A/C with the MLGD open and provided the necessary inputs for the FEM update. The adjustment of the numerical model allowed to match well the first two modes. Anyway, it was difficult to achieve a good correlation of the third elastic mode, which presented a MAC of 65.6% after the model update.

Aquilini *et al.* [4] provided the theoretical background for the CFD-CSM one way coupling. Spectra of the MLGD actuator force and accelerations on four points of the door were computed and compared with the flight test measurements. Results provided a good matching, especially when comparing the actuator force RMS values, with deviations of only 2.4% with respect to flight test measurements. Acceleration levels were also well predicted, with differences between 0.6% and 12% with the flight test results, except for the hinge line location. This was expected, since the third elastic mode, which has the biggest influence on this location, was poorly matched with the GVT results. Excluding the third mode from the modal base and repeating the buffeting analysis sensibly improved the results.

The aforementioned numerical studies were a fundamental stepping stone for the design of three different devices: VGs, deflectors and a spoiler were manufactured and finally flight-tested. Extensive flight test preparation described by Schwochow *et al.* [3] was conducted. Special care was taken to ensure that for all flight points each device could be compared with the associated clean configuration, under similar flight conditions.
The VGs installed on the MLGD outer surface presented performances up to 10.6%, comparing the actuator RMS forces with the baseline configuration. The RMS of the accelerations at the door tip were up to 40% lower with respect to the clean configuration. No appreciable dependency with the flight speed was found.
The deflectors were installed on the doors leading edges at the inner face. They provided actuator RMS forces up to 12.5% lower with respect to the clean configuration at high flight speeds. The analysis of the RMS evolution over time showed a stable behaviour with a small dependency with the flight speed (reductions up to 9.7% at low flight speeds were identified).
The spoiler, a lifting surface which reduces the MLGD tendency to open, provided actuator RMS force reductions up to 11.2%, at high flight speeds. However, the results were highly dependent from the flight speed, resulting almost ineffective at low speeds.

8 ACKNOWLEDGEMENTS

The work described in this paper and the research leading to these results have received funding from the European Community's Seventh Framework Programme FP7/2007-2013, under grant agreement n° 604013, AFLONEXT project. The authors are particularly grateful to partners involved in WP 3 for all interesting discussions during the project meetings.

http://www.aflonext.eu/
https://www.youtube.com/watch?v=iNFtSg8x6Vc&feature=youtu.be

9 REFERENCES

[1] Peng, S.-H., Jirasek, A., Dalenbring, M. and Eliasson, M., Aerodynamic excitation on MLG door exposed to vortices emanating from NLG of an aircraft model. AIAA Paper 2016-4043. AIAA Aviation 2016. Washington DC, 13-17 June 2016.

[2] Tomac, M., A. Rizzi, D. Charbonnier, J.B. Vos, A. Jirasek, S-H. Peng, A. Winkler, A. Allen, G. Wissocq, G. Puigt, J. Dandois, R. Abarca. Unsteady Aero-Loads from Vortices Shed on A320 Landing Gear Door: CFD compared to fight tests. . AIAA Paper 2016-0803.

[3] Schwochow, J., Sinske, J., Buchbach, R. (2018). Inflight-Measurements of Aircraft Undercarriage Vibration during Deployment. *In: proceedings of the European Test and Telemetry Conference 2018*, Nürnberg, Germany. ISBN 978-3-9816876-8-2.

[4] Aquilini, C. and Parisse, D. (2017). A Method for Predicting Multivariate Random Loads and a Discrete Approximation of the Multidimensional Design Load Envelope. Como: IFASD 2017

[5] Albano, E. and Rodden, W. P. (1969). A doublet-lattice method for calculating lift distributions on oscillating surfaces in subsonic flows. AIAA Journal, 7(2), 279–285.

[6] Rodden,W. P. and Johnson, E. H. (1994). MSC.Nastran Aeroelastic Analysis Users Guide Version 68, p.71.

[7] Schwochow, J., Sinske, J., Buchbach R., Govers, Y., Abarca-Lopez, R. (2019). Operational Modal Analysis of Moving Airfraft Landing Gear Doors in Flight. *In IOMAC 2019 - 8th International Operational Modal Analysis Conference*. Copenhagen, Denmark

10 NOMENCLATURE

A/C	aircraft
AFLoNext	Active Flow- Loads & Noise control on Next generation wing
AoA	angle of attack
CFD	computational fluid dynamics
CSM	computational structural mechanics
FEM	finite element model
FRF	frequency response function
FT	flight test
FTI	flight test instrumentation
GVT	ground vibration test
LES	large eddy simulation
LG	landing Gear
MAC	modal assurance criterion
MLG	main landing gear
MLGD	main landing gear door
NLG	nose landing gear
PRM	phase resonance method
PSD	power spectral density
PSM	phase separation method
RANS	Reynolds averaged Navier-Stokes
RMS	root-mean-square
VC	vibration control
VGs	vortex generators

COPYRIGHT STATEMENT